

# Mapping and characterization of rock discontinuities in a tunnel using 3D terrestrial laser scanning

Pedro Pazzoto Cacciari<sup>1</sup> · Marcos Massao Futai<sup>1</sup>

Received: 17 June 2014 / Accepted: 13 April 2015 / Published online: 29 April 2015  
© Springer-Verlag Berlin Heidelberg 2015

**Abstract** This paper attempts to evaluate various methods of geometrical discontinuity characterization using point clouds that are generated with three-dimensional terrestrial laser scanning (3DTLS) in a tunnel. The use of 3DTLS to support discontinuity mapping in tunnels enables the acquisition of a large amount of data without limitations in terms of the tunnel position (wall or roof). Thus, the discontinuity orientation, trace length and frequency were statistically analyzed in different regions of the tunnel to determine the most representative data. Different methods of estimating the mean trace length were compared while considering the variations in the rock face orientation in the tunnel, and the unbiased standard deviation of the trace length was evaluated. The frequencies of discontinuity sets were obtained using scanlines, and aspects of window sampling for density (areal frequency) estimates in tunnels are discussed. The mean trace lengths obtained using rectangular sampling windows (considering the relative frequency of the traces) are more suitable for estimates of different rock face orientations, particularly when the orientation of the discontinuity set varies significantly. In this case, measurements of samples from the tunnel roof presented higher values for both frequency and mean trace length estimates, which demonstrates the importance of data acquisition and evaluation in this region.

**Keywords** Discontinuity · Laser scanner · Mean trace length · Frequency · Tunnel

## Introduction

The complex mechanical behavior of a rock mass is strongly influenced by geological structures such as joints, faults and foliations. Thus, an important aspect concerning the evaluation of a rock mass is the geometrical characterization of discontinuities. Rock discontinuities can be analyzed in the field using various standard methods (ISRM 1978). However, several issues can often complicate manual geological data acquisition (i.e., bed access to rock faces and absence of illumination), and these sampling difficulties lead to erroneous or insufficient data.

Considering these difficulties, several authors (Crosta 1997; Kemeny et al. 2006; Strouth et al. 2006; Slob et al. 2007; Haneberg 2008; Ferrero et al. 2009; Sturzenegger and Stead 2009; Lato et al. 2010; Mah et al. 2011; Sturzenegger et al. 2011) have studied alternative methods of geological-discontinuity mapping and characterization based on 3D images, which are obtained using both 3D terrestrial laser scanning and digital photogrammetry. More specifically, for tunneling, Fekete et al. (2010) showed many applications of 3D terrestrial laser scanning (3DTLS), including rock discontinuity mapping.

Several old tunnels along Brazilian railways were constructed in jointed rock masses with no concrete liners or both liners and bolts. In the past few years, some of these tunnels have shown localized stability problems (with sporadic block falls), which demand a reevaluation of the rock mass quality at certain critical areas. The *Vitória-Minas* railway in *Espirito Santo* state in southeastern Brazil has 22 tunnels in this condition, and the intense rail traffic

✉ Pedro Pazzoto Cacciari  
ppazzoto@gmail.com

<sup>1</sup> Geotechnical Engineering Department, Polytechnical School, University of São Paulo, Av. Prof. Luciano Gualberto, travessa 3 no 380, Cidade Universitária, Butantã, São Paulo, SP CEP 05508-010, Brazil

(cargo and passengers) reduces the timeframes available for inspections (geological mapping and geomechanical evaluations). The lengths of these tunnels vary from hundreds of meters to a few kilometers, which makes conventional field discontinuity mapping a strenuous and time-consuming task when a detailed analysis is required. In addition, when using conventional geological mapping in tunnels, it is difficult to obtain the actual position and geometrical parameters (generally given as orientation, frequency and trace length) of all discontinuities, mainly in the higher regions of the tunnel section.

Using 3D images (e.g., 3DTLS point clouds), it is possible to perform geometrical discontinuity characterization on any part of the tunnel section with the same level of detail, which allows the verification of geometrical-parameter variations for different orientations of the rock face (i.e., tunnel roof and walls). Here, the 3DTLS point cloud technique is used to perform geometrical discontinuity analysis in a fractured tunnel of the *Vitória-Minas* railway to verify the applicability of different methods of estimating the mean trace length and frequency considering the variations in orientation in a tunnel rock face.

### 3DTLS data acquisition

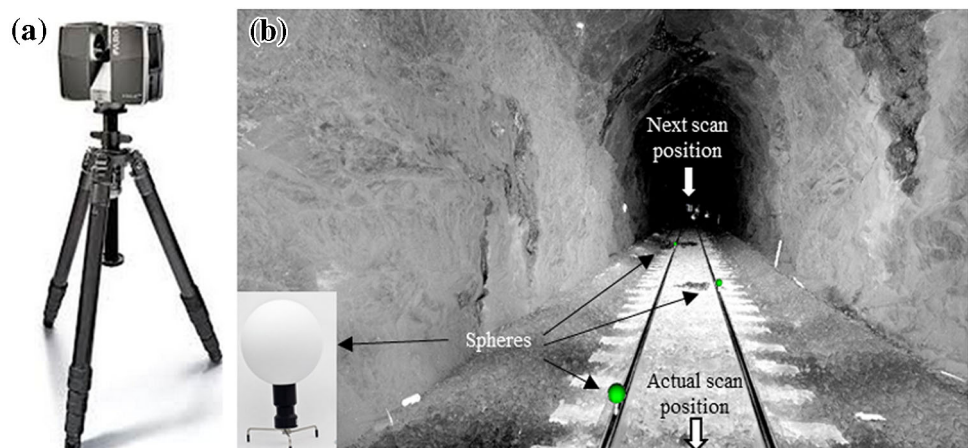
In this study, we used the Faro Focus 3D laser scanner (Faro Inc. 2013; Fig. 1a). This instrument operates at a measurement speed of 976,000 points/second with a distance accuracy of approximately 2 mm. The spacing between scan stations was 10 m with a 360° rotation time of 7.3 min. The obtained point clouds in each scan were aligned using the superposition of three fixed spheres (Fig. 1b) that could be produced using each pair of consecutive scans. This alignment procedure is easily performed when using the automatic recognition of objects

(spheres in this case), which is a feature available in the Scene 5.0 software (Faro Inc. 2013). The resulting file, which contains all point clouds (after the scan alignment), has a size on the order of dozens of gigabytes; thus, it is usually necessary to use powerful workstations to manipulate the images. Figure 1b shows a view of the point cloud that was obtained from the studied tunnel.

### Quality of the point cloud

The high measuring rates of certain currently available 3DTLS instruments can be used to produce high-resolution images (high-density point clouds). However, objects that are not in the lines-of-sight of the scanner cannot be imaged, and blank regions in the point clouds are thus generated (occlusions). A large number of occlusions typically result in low-quality point clouds (Lato et al. 2010). Outcrops of fractured rock are generally notably irregular and form acute angles between discontinuities. Therefore, depending on the orientation between the lines-of-sight and the rock face, zones with an absence of points (occlusion) are formed; specifically, when the line-of-sight and the rock face have similar orientations, regions of fair visibility may be generated (Lato et al. 2010). A large number of these occlusions are eliminated when subsequent scans are aligned, but certain occlusions cannot be viewed along the lines-of-sight at any position (where the instrument can be fixed) in the tunnel, which results in a few occlusions in the final image. Figure 2 shows a point cloud section of the tunnel with two examples of occlusion and the mean dimensions of the excavation, where the height and width vary by approximately 50 cm as a result of irregularities along the tunnel. Here, the previously described planning data acquisition generated a point cloud with only a few small remaining occlusions (no greater than the indicated amount in Fig. 2).

**Fig. 1** **a** Faro Focus 3D laser scanner and spheres used for alignment, **b** final point cloud of the tunnel with two consecutive scans with identical recognizable spheres



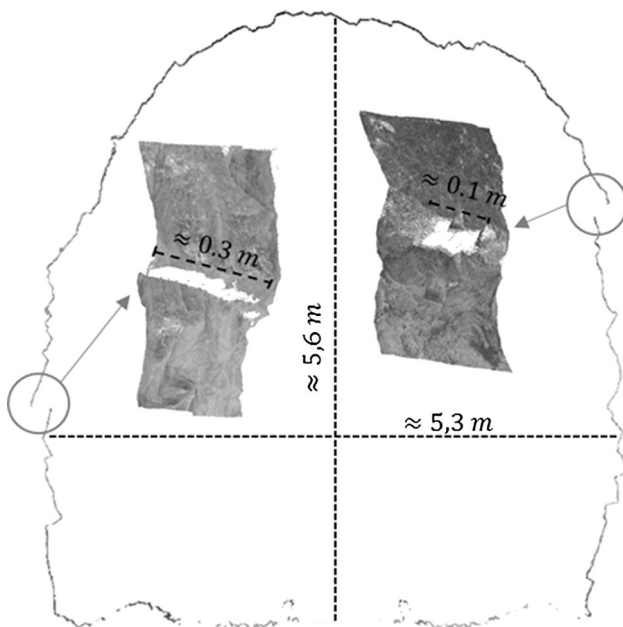


**Fig. 2** Section of the point cloud with two occlusion examples and an indication of the mean height ( $\approx 5.6$  m) and width ( $\approx 5.3$  m) of the tunnel

### Discontinuity mapping in the point cloud

Identification of the discontinuity planes in the point cloud consists of finding systematic coplanar regions of the cloud and computing the normal vector (described by 3-direction cosines and an  $xyz$  origin) and the length of each region as a plane. Recently, several authors (Kemeny et al. 2006; Lato et al. 2009; Gigli and Casagli 2011; Lato and Vöge 2012; Umili et al. 2013) developed methods of automatic discontinuity recognition in point clouds or digital models that are generated by such point clouds. All of these methods assume that the discontinuities are coplanar regions in the images, which allows the algorithms to automatically recognize them. The most recent automatic methods, which were published by Lato and Vöge (2012) and Umili et al. (2013), appear promising; however, they remain in the developmental stage.

Here, the manual method is applied, which consists of inspecting the point cloud, fitting the planes in coplanar regions and taking length measurements (Fig. 3), using Spilt-FX software (Split Engineering, LCC. 2007) to measure orientations and Scene 5.0 software to measure trace lengths. In the 3DTLS survey, the discontinuity planes are individually described using the same parameters as in hand-made field geological surveys. Using the direction cosines of normal vectors, along with simple algebra, it is easy to obtain the discontinuity orientation (normally described in dip $^\circ$  and dip direction $^\circ$  for engineering purposes).

In most cases, only small areas of discontinuities are exposed in a rock face, which makes it difficult or even impossible to determine the areal size of the planes. Thus, the trace length (length of the intersection between a joint plane and the rock face) is usually adopted to describe the discontinuity sizes. Considering that all points in point clouds are in a metric Cartesian coordinate system, it is possible to measure the trace lengths using a measuring tape as in conventional hand mapping. Figure 3 shows a small portion of the obtained point cloud from the tunnel, which demonstrates the trace length measurements (Fig. 3a), and the coplanar points of the fractures that were used to determine the orientation (Fig. 3b).

### Sources of bias in 3DTLS discontinuity mapping in tunnels

As verified by Lato et al. (2010), there are several sources of bias when using 3DTLS for geological structural mapping. The most relevant factor for obtaining satisfactory results when performing a geometrical discontinuity characterization is the level of exposure of the planes. In tunnels, this level can increase or decrease depending on the damage to the rock face, which is a function of the type of excavation (blasting, cutting, etc.) and weathering. In addition, the plane exposure in fractured rocks depends on the number and volume of failed blocks, which varies with the strength and geometry characteristics of each discontinuity set and the level of disturbance caused by the excavation type. Certain aspects of these sources of bias are separately discussed below.

#### Orientation Bias

This orientation bias refers to the fact that when the discontinuity surface normal ( $N_D$ ) becomes increasingly parallel to the rock face normal ( $N_{RF}$ ), the observed spacing of the apparent traces ( $D_a$ ) on the outcrop increases with respect to the perpendicular (true) spacing ( $D_p$ ) (Fig. 4). Terzaghi (1965) first proposed correction of this bias using a discontinuity correction factor that varies with the sine of the angle ( $\beta$ ) between  $N_{RF}$  and  $N_D$ , as shown in Fig. 4. The inverse of the correction factor can be used to calculate the true spacing of the discontinuity planes. When the orientation bias decreases the occurrence probability of a discontinuity set on a rock face, it directly affects the mean geometrical parameters to be estimated (dip, dip direction, spacing and length). In tunnels, the effect of the orientation bias must be analyzed for each discontinuity set considering the variation in the rock face normal in each part of the section (walls and roof).

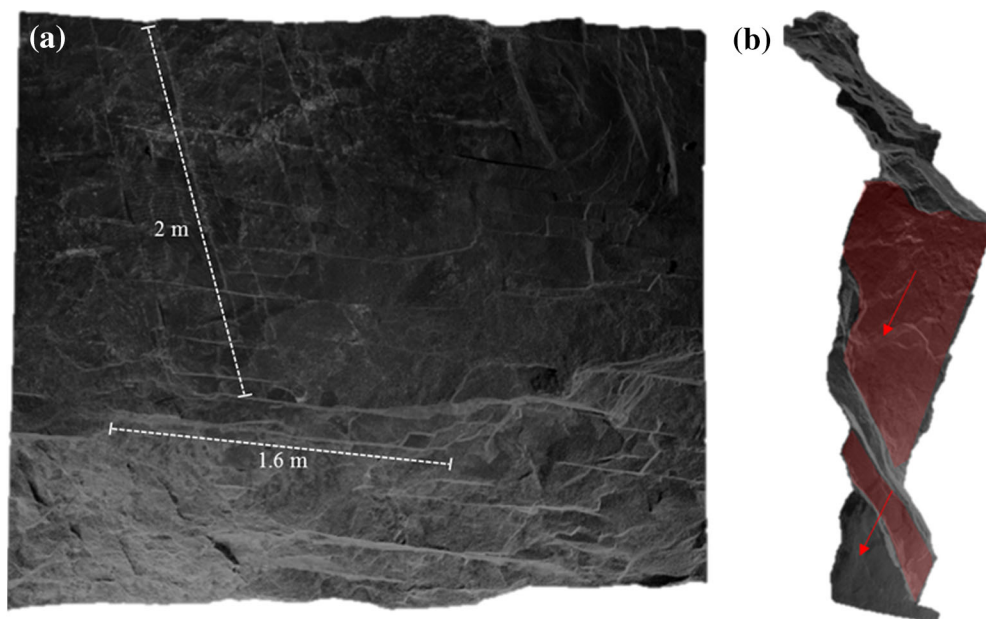


**Fig. 3** Identification of discontinuities in point clouds. **a** Obtaining the trace length of the planes, **b** obtaining the orientation of the planes

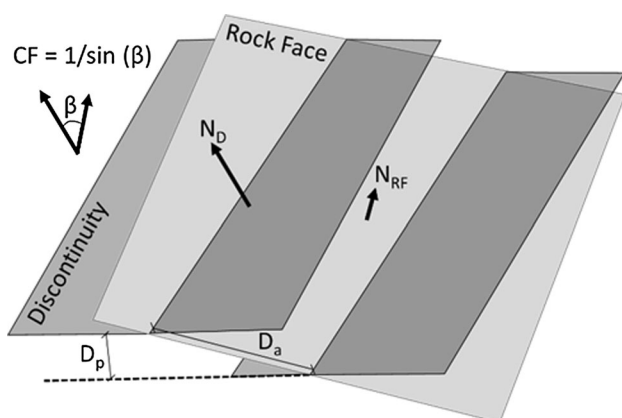


**Fig. 4** Effect of orientation bias on discontinuity sampling and the Terzaghi correction factor

#### Limited exposure

Even with the high technology of 3DTLS instruments, discontinuity planes with non-exposed areas in the rock face are poorly identified in the point cloud. Discontinuities with a small exposure (on the order of millimeters) or a sufficiently thick filling or aperture (on the order of millimeters) can be identified, but the measurement of the orientation will be hindered. Figure 5 shows an example of different cases of limited exposure in an arbitrary portion of the point cloud (representing the tunnel's east wall) with six apparent discontinuities from a single set. In this case, the analyzed set dips perpendicularly to the tunnel axis (Fig. 5a), and limited exposures are expected. Figure 5a

shows the orientations (poles) of the ten best exposures of identical discontinuities in Fig. 5b (not necessarily only one measurement per discontinuity), which indicate the mean orientation and variability. The profiles in Fig. 5c (obtained from cross sections A–D in Fig. 5b) indicate that not all apparent traces in the point cloud (1–6) have at least one good exposure (i.e., fractures 1 and 2) for use when determining the orientation, but their traces can still be identified and measured. Therefore, considering the orientation variability (i.e.,  $16.7^\circ$ ), in cases such as fractures 1 and 2 in Fig. 5, it is reasonable to assume the mean orientation that is obtained using the stereographic analysis. Moreover, using 3DTLS mapping, it is difficult to correlate every trace length measurement with an orientation and, thus, potentially leading to biases.

#### Discontinuity analysis

Various geometrical discontinuity analysis techniques (Kulatilake and Wu 1984a; Mauldon 1998; Zhang and Einstein 1998, 2000; Wu et al. 2011) are tested in an 8-m-long part of a 970-m-long tunnel from the *Vitória-Minas* railway. This tunnel was constructed in foliated gneiss from the *Paraíba do Sul* complex, which is part of the *Araçuaí* Paleoproterozoic orogenic belt. The 8-m section of the tunnel was chosen because of the high number of fractures identified during the field inspection and in the point cloud. With this section of the tunnel as an example, we aim to verify the applicability of different discontinuity characterization methods, considering the difficulties posed



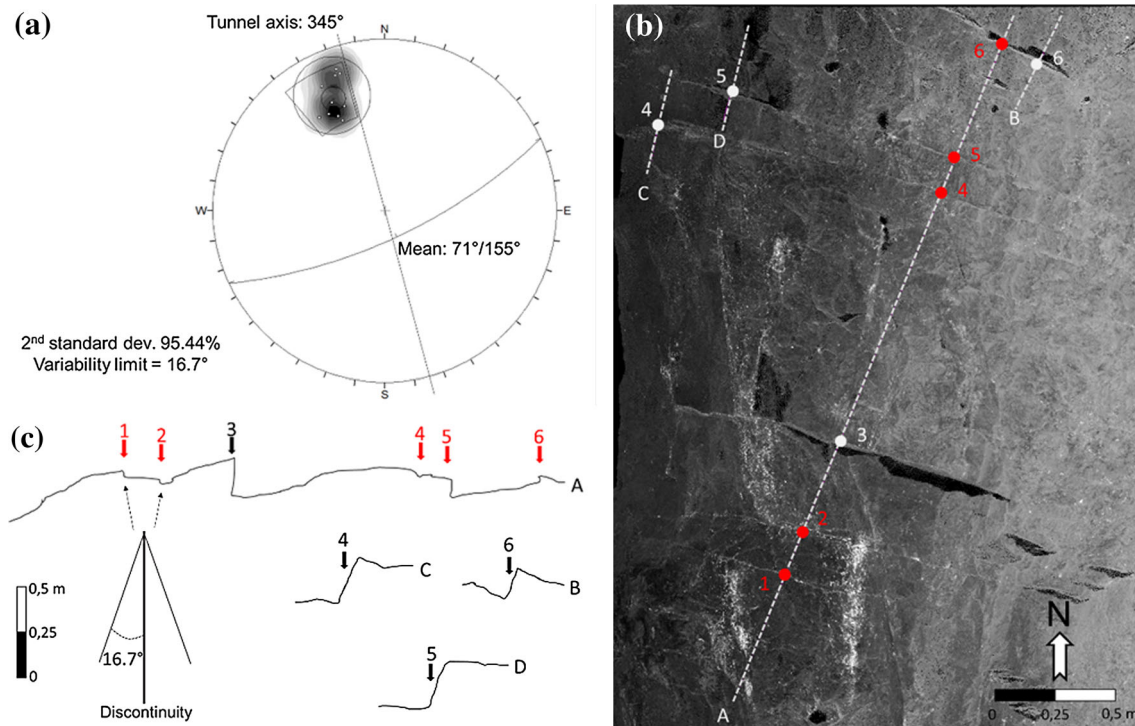


**Fig. 5** **a** Stereonet with pole concentrations of the fractures (1–6), **b** region of the point cloud from the east wall of the tunnel with six visible fractures and four indicated cross sections (A–D), **c** profiles of the cross sections (A–D)

by limited space and rock face curvature in underground excavations.

The geometrical characterization of a discontinuity set can be summarized using three parameters, orientation, trace frequency and mean trace length; thus, these parameters will be obtained and discussed below.

### Orientation

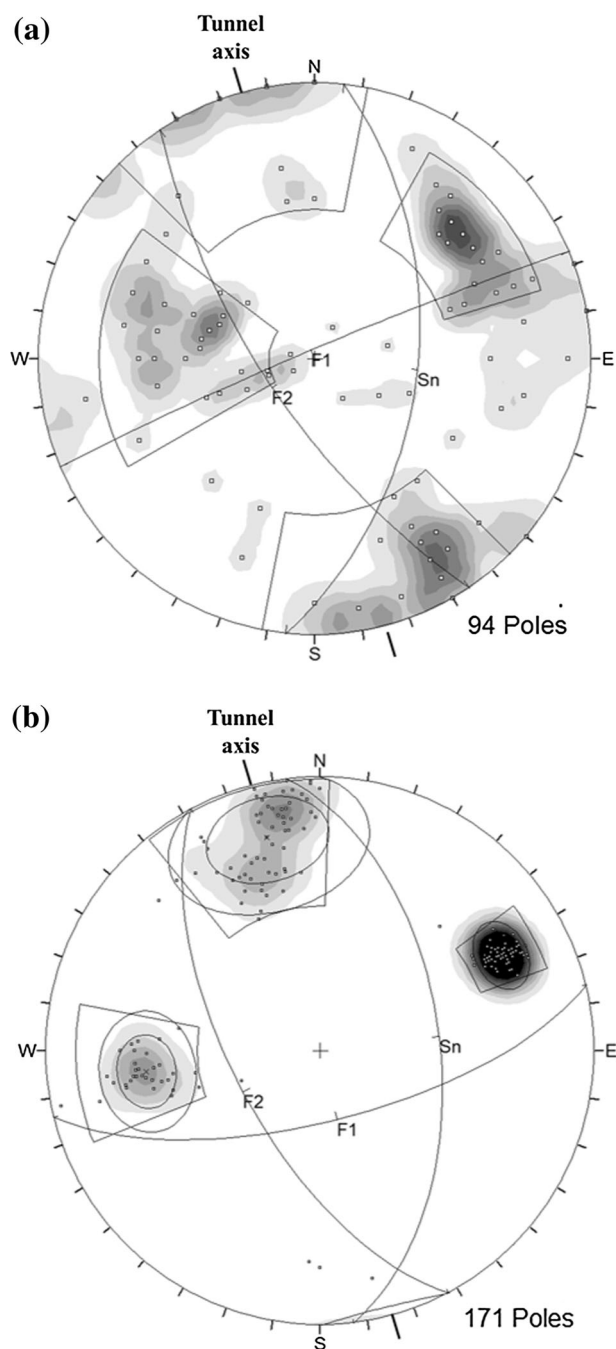
The orientations of discontinuities are presented in stereonet plots as poles and contours. Several authors (Kemeny et al. 2006; Sturzenegger and Stead 2009; Fekete et al. 2010; etc.) have manually inspected and shown the similarity of the orientation data that were obtained from hand-made mapping (with geological compass) and from 3DTLS image mapping. Figure 6 shows the results generated using orientation data obtained for the 8-m-long section of the tunnel (3DTLS) and a previous hand-made mapping that was made during a 2-h field inspection along the entire length of the tunnel. Because the field data acquisition (Fig. 6a) was randomly performed along a length of 970 m, the data were expected to include greater variability compared to data obtained using localized 3DTLS mapping (Fig. 6b). However, it is possible to recognize similar patterns in both stereograms with three well-defined discontinuity sets, in which one set is the rock foliation ( $S_n$ ) and the remaining two sets are fracture sets ( $F_1$  and  $F_2$ ).

Figure 6 also shows the tunnel axis, which indicates that the  $S_n$  (dipping E) and  $F_2$  (dipping WSW) strikes are approximately parallel to the tunnel axis, and  $F_1$  (sub-vertical dipping SSE and NNW) is nearly perpendicular to the tunnel axis. Table 1 summarizes the mean orientations and statistical characteristics of the discontinuity sets in Fig. 6b, analyzed using DIPS (Rocscience Inc. 2006).

A discontinuity analysis is separately performed for each type of geological structure that was identified in the tunnel. Two fracture sets are analyzed as impersistent structures to investigate the set frequency and mean trace length (persistence). The rock foliation in the gneiss results from the parallel-planar alignment of platy mineral grains (mostly biotite) during metamorphism, which may be observed at several scales (from satellite images to microscopic petrography). Considering the genesis of these structures, the authors believe that it may be risky to estimate a mean length and frequency for  $S_n$  based on images of the tunnel rock face. Therefore, the foliation analysis is restricted to the orientation.

### Trace length

The size of discontinuities is an important but difficult parameter to determine. In rock outcrops, because only the traces can be measured, the discontinuity areal size and shape must be inferred from the trace lengths. Nevertheless, a



**Fig. 6** Stereograms (lower hemisphere, Fisher concentrations) of discontinuity poles. **a** Hand-made mapping of the entire tunnel, **b** 3DTLS mapping of the 8-m-long section of the tunnel

**Table 1** Characteristics of the identified discontinuity sets

Set	No. of poles	Dip (°)	Dip dir. (°)	<i>K</i> (Fisher)	1st Standard deviation (SD; °)	2nd SD (°)
<i>S<sub>n</sub></i>	31	54	80	78.9	9.8	16.0
<i>F<sub>1</sub></i>	70	69	166	32.8	15.2	25.1
<i>F<sub>2</sub></i>	62	64	242	251.3	5.5	8.9

representative trace length for a discontinuity set (mean trace length) cannot be obtained from direct measurements of the traces in the rock face because of biases (e.g., censoring and size bias), which have been discussed by several authors (Cruden 1977; Baecher 1980; Pahl 1981; Kulatilake and Wu 1984a; Priest 1993; Mauldon 1998; Zhang and Einstein 1998). The estimation of an unbiased mean trace length has been of great interest in the literature; some of the suggested methods are applied in this study. Kulatilake and Wu (1984a) suggested the following equations to estimate an unbiased mean trace length ( $\mu$ ):

$$\mu = \frac{wh(1 + R_0 - R_2)}{(1 - R_0 + R_2)(wB + hA)} \quad (1)$$

$$A = \int_{\alpha_l}^{\alpha_u} \int_{\psi_l}^{\psi_u} |\cos \varphi| f(\psi, \alpha) d\psi d\alpha \quad (2)$$

$$B = \int_{\alpha_l}^{\alpha_u} \int_{\psi_l}^{\psi_u} \sin \varphi f(\psi, \alpha) d\psi d\alpha \quad (3)$$

where  $w$  is the width,  $h$  the height of a rectangular window;  $R_0$  and  $R_2$  are the fractions of transecting (both ends censored) and contained (both ends observable) traces, respectively;  $\psi$  is the dip°;  $\alpha$  is the dip direction°;  $f(\psi, \alpha)$  is the probability density function;  $l$  and  $u$  are the lower and upper limits of the orientation, respectively; and  $\varphi$  is the apparent dip of discontinuities in a vertical sampling plane. The application of Eq. 1 can be complicated because of the difficulty in determining the distribution forms of  $f(\psi, \alpha)$  and finding the parameters  $A$  and  $B$ . Thus, Wu et al. (2011) proposed the following approximations for  $A$  and  $B$ :

$$A \approx \sum_{i=1}^N [|\cos \varphi_i| \times \text{Rf}(\varphi_i)] \approx E(\cos \varphi) \quad (4)$$

$$B \approx \sum_{i=1}^N [\sin \varphi_i \times \text{Rf}(\varphi_i)] \approx E(\sin \varphi) \quad (5)$$

where  $\varphi_i$  and  $\text{Rf}(\varphi_i)$  are the apparent dip and relative frequency of the  $i$ th discontinuity, respectively. The procedure to calculate  $\text{Rf}(\varphi_i)$  depends on a weighting function and is described in detail in Wathugala and Kulatilake (1990) and Wu et al. (2011).

Mauldon (1998) developed an estimator of the mean trace length for windows with arbitrary convex boundaries and demonstrated the estimator using two examples. The first case was for rectangular windows, which is similar to the estimator in Eq. 1 but does not depend on a probability distribution function (after all traces are considered parallel,  $A$  and  $B$  in Eqs. 2 and 3 assume deterministic values). The second case is for circular windows, where the symmetry of the shape allows for an estimate of  $\mu$  for non-parallel traces. Zhang and Einstein (1998) also found an expression that is identical to that of Mauldon (1998) for circular windows:

$$\mu = \frac{\pi r (N + N_T - N_C)}{2 (N - N_T + N_C)} \quad (6)$$

where  $r$  is the radius of a circular window,  $N$  is the total number of observed traces, and  $N_T$  and  $N_C$  are the numbers of transecting and contained traces, respectively. Mauldon et al. (2001) proposed that an average of several  $\mu$  values obtained from Eq. 6 for an identical window radius could be estimated as

$$\mu = \frac{\pi r \bar{n}}{2 \bar{m}} \quad (7)$$

where  $n = (N + N_T - N_C)$  and  $m = (N - N_T + N_C)$  for each sampling window.

Moreover, Zhang and Einstein (2000) proposed an estimate of the unbiased SD ( $\sigma$ ) using the covariance of measured trace lengths ( $\text{COV}_m$ ):

$$\sigma = \mu(\text{COV}_m) \quad (8)$$

Thus, as suggested by Zhang and Einstein (2000), once the measured trace length distribution function is known, an identical distribution form can be assumed for the true

(unbiased) trace lengths, the mean and SD of which are given by Eqs. 6 and 8.

Table 2 summarizes important characteristics, with respective advantages and disadvantages, of the previously described mean trace length sampling methods.

All observable discontinuity traces ( $F_1$  and  $F_2$  sets) in the point cloud were mapped and measured in the same part of the tunnel (8-m-long section, as shown in Fig. 7a) previously used for the orientation analysis (Fig. 6). Figure 7b represents the result with the identified traces in each component of the tunnel (walls and roof) using the 3DTLS point cloud. The first observation from Fig. 7b is that the west wall has fewer mapped traces compared to the other two regions because of the orientation of the  $F_2$  fractures (orientation bias) and a block failure in this section of the tunnel, which will be discussed later in greater detail. To obtain the best characterization of the discontinuity geometry in the tunnel, the windows were only sampled on the east wall and roof.

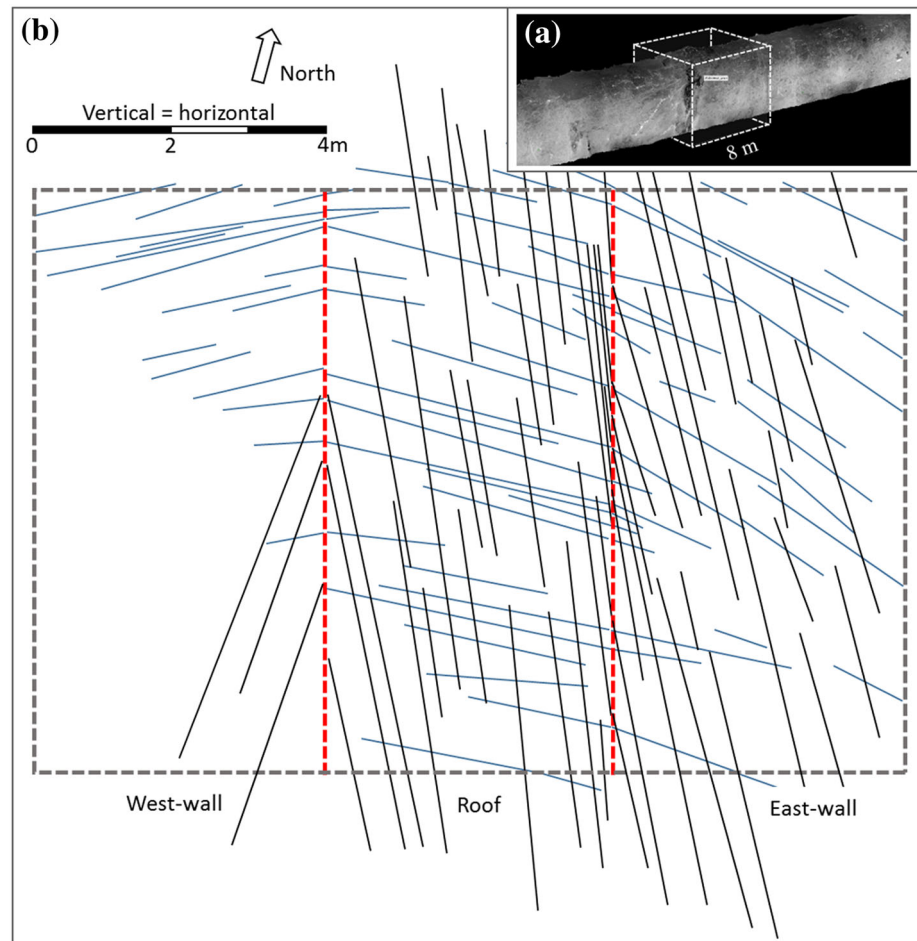
All sampling windows were analyzed in the trace map of Fig. 7b. The wall and roof extension limits the sampling area, which is a problem associated with applying window sampling in tunnels. Therefore, when using a circular window, the window diameter cannot be larger than the vertical length of the walls or the horizontal length of the roof (perpendicular to the tunnel axis). This issue can result in two different problems:

1. If the traces exceed the maximum window diameter, an excessive number of transecting traces will appear in the window, which leads to an overestimation of the mean trace length. As described by Zhang and Einstein (1998), if all traces transect the window, then  $\mu \rightarrow \infty$ .
2. If the walls or the roof are longer in one direction than in the other (as in Fig. 7b), a single circular window

**Table 2** Characteristics of the mean trace length sampling methods

Method	Window type	Distribution-free method	Applied to non-parallel traces	Considers relative frequencies of traces depending on the rock face orientation
Kulatilake and Wu (1984a)	Rectangular	No (depends on the definition of the $f(\psi, \alpha)$ function)	Yes	Yes
Mauldon (1998)	Any convex	Yes	No	Yes (but only when traces are essentially parallel, thus enabling one to assign deterministic values for $A$ and $B$ )
Mauldon (1998), Zhang and Einstein (1998)	Circular	Yes	Yes	No
Wu et al. (2011)	Rectangular	Yes (with a numerical approximation of $A$ and $B$ )	Yes	Yes

**Fig. 7** **a** Tunnel point cloud and the selected area, **b** trace map that resulted from the 3DTLS mapping



cannot represent the entire area, which forces one to use an average of several circular samplings aligned in the longer direction.

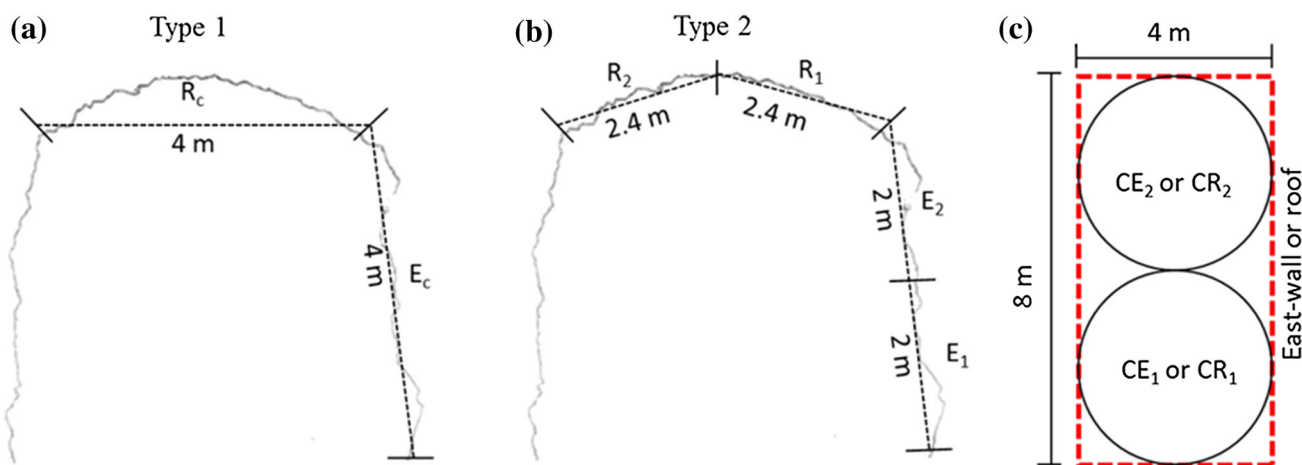
Problem number 2 can be directly avoided using rectangular sampling windows. Problem number 1 can be minimized depending on the trace orientation. Extreme situations can occur if the traces are parallel to the tunnel axis (similar to  $F_2$ ), whereby the width of a rectangular sampling window on the roof or the walls can be increased as much as necessary. If the traces are perpendicular to the tunnel axis (similar to  $F_1$ ), then the rectangular sampling window has the identical size limitation of a circular window. However, in cases whereby most discontinuities of a given set transect, the discontinuities can be considered as persistent planes on the scale of the tunnel diameter; hence, a mean trace length estimate may not be necessary depending on the application.

Considering these problems, rectangular sampling windows are used here to estimate the mean trace length of fractures  $F_1$  and  $F_2$  following the methods proposed by Kulatilake and Wu (1984a) and Wu et al. (2011) and using Eqs. 1, 4 and 5. Circular sampling windows (Eq. 6) are

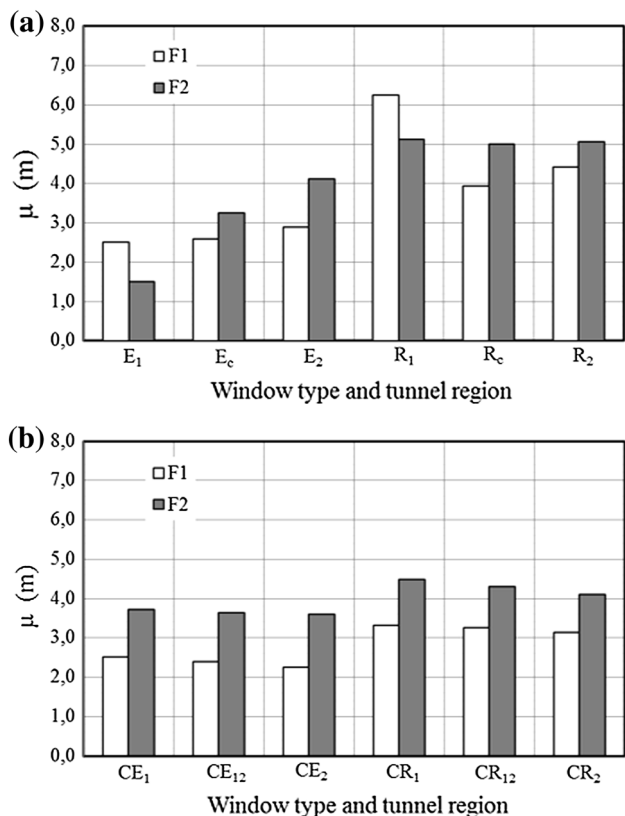
also used for comparison. As previously described, the angle  $\varphi$  in Eqs. 4 and 5 represents the apparent dip of a discontinuity that appears in a vertical sampling plane. However, the apparent dip of a trace is a particular case of the trace rake. Therefore, when the tunnel section is subdivided into multiple planar and non-vertical surfaces (Fig. 8a, b), the traces that appear in each surface have different rakes ( $\varphi$ ). Using 3DTLS point clouds for the discontinuity orientation measurements, all (sufficiently exposed) planes can be measured independently of the tunnel region. Thus, Eqs. 4 and 5 can be separately applied to each region of the tunnel (sub-divisions in Fig. 8) for each discontinuity set. Not all discontinuities with measured traces (Fig. 7b) had their orientation measured because of the limited number of exposures (Fig. 5); however, in larger traces, with more than one good exposure, the orientation was also measured more than once.

Figure 8 shows the methodology used to separate the tunnel section into planar surfaces. All resulting rectangular windows are 8 m wide, and the height varies according to the sub-division. Two types of sub-divisions were adopted: type 1 (Fig. 8a), with only two divisions





**Fig. 8** Sub-division of the tunnel section used to apply rectangular and circular window sampling. **a** Sub-division type 1 indicates the variation in window height, **b** sub-division type 2 indicates the variation in window height, **c** circular windows were adjusted on the east wall or roof



**Fig. 9** **a** Mean trace length ( $\mu$ ) estimated with rectangular sampling windows, **b** mean trace length ( $\mu$ ) estimated with circular sampling windows

(complete east-wall  $E_c$  and complete roof  $R_c$ ), and type 2 (Fig. 8b), with four divisions ( $E_1$ ,  $E_2$ ,  $R_1$  and  $R_2$ ). Circular windows were adjusted only in  $R_c$  and  $E_c$  (sub-division type 1), as indicated in Fig. 8c.

Figure 9a show the estimated mean trace lengths ( $\mu$ ) with rectangular sampling windows using Eq. 1 for all sub-

divisions in Fig. 8a and b and with  $A$  and  $B$  obtained from Eqs. 4 and 5 for these sub-divisions. Figure 9b shows the estimated mean trace lengths with circular sampling windows using Eq. 6 and the average of each pair of samples (denoted by  $CE_{12}$  or  $CR_{12}$ ) using Eq. 7. Figure 9 shows that the values of  $\mu$  that were obtained for the roof are higher than those for the east wall for both  $F_1$  and  $F_2$ , and this difference is more evident in Fig. 9a for rectangular sampling windows. This result indicates that the mapped traces in the roof tend to be more continuous than in the east wall. The value of  $\mu$  that was obtained for  $F_1$  in the rectangular window  $R_1$  is different from other samples of the roof. This value is most likely an overestimation of the trace length because of the small height of  $R_1$ , which results in an excessive number of transecting  $F_1$  traces.

For the unbiased SD ( $\sigma$ ) estimate, the covariance of the measured trace lengths ( $COV_m$ ) must be known, as suggested by Zhang and Einstein (2000). In this reference, the author found this relation by measuring the length of the traces in circular windows of different areas (only the portions of the traces within the windows) and calculating the mean ( $l_m$ ) and SD ( $\sigma_m$ ) of the measured trace lengths. For rectangular windows, there should be an identical correlation, but it is important to verify the consistency of the  $COV_m$  values in different rectangular areas. In this study, to perform this analysis,  $l_m$  and  $\sigma_m$  were calculated for different areas for  $F_1$  and  $F_2$ , as indicated in Fig. 10a. With these sub-divisions,  $l_m$  and  $\sigma_m$  were calculated in eight windows of  $8\text{ m}^2$ , four windows of  $16\text{ m}^2$ , and two windows of  $32\text{ m}^2$  for  $F_1$  and  $F_2$ . Figure 10b shows the result of this analysis, where each value of  $\bar{l}_m$  and  $\bar{\sigma}_m$  for  $F_1$  and  $F_2$  is an average of all of the values obtained for each window area. The results indicate that an identical relation found by Zhang and Einstein (2000) can be used in this case for rectangular sampling windows, and the  $COV_m$

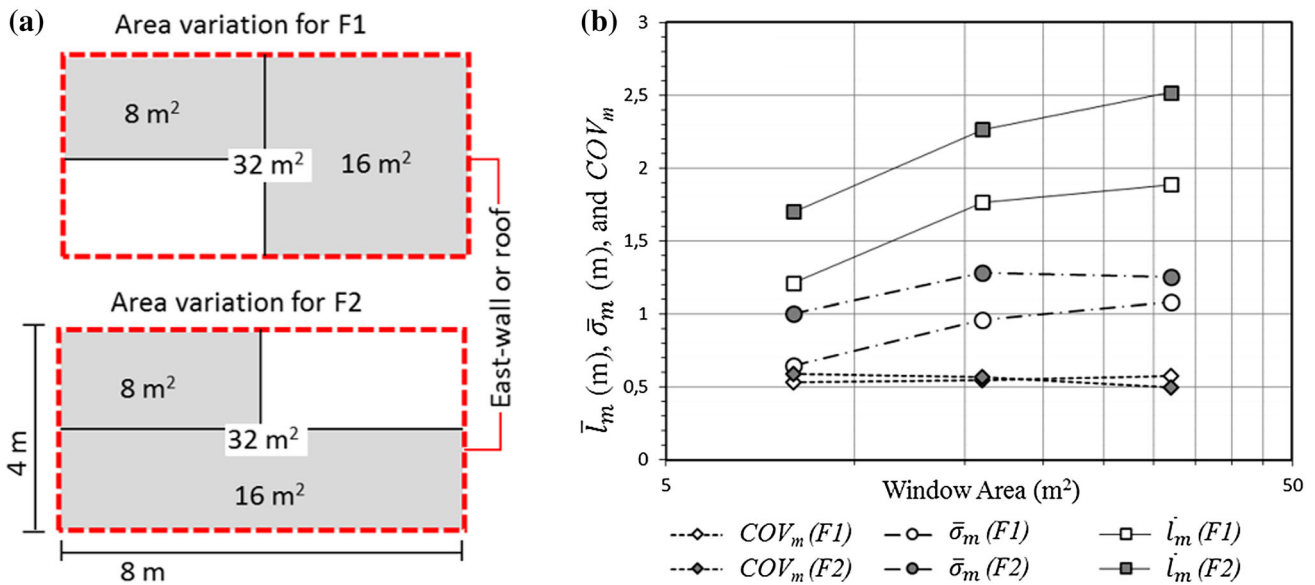


**Fig. 10** a Areal variations of the rectangular windows for the  $COV_m$  analysis, b measured trace length ( $\bar{l}_m$ ), SD ( $\bar{\sigma}_m$ ) and covariance ( $COV_m$ ) for  $F_1$  and  $F_2$

value is practically identical for  $F_1$  and  $F_2$  (approximately 0.5 in this case). Thus, the obtained  $COV_m$  indicates that the unbiased SD ( $\sigma$ ) in this case can be considered as approximately half of the mean trace length ( $\mu$ ) for all presented estimates in Fig. 9a.

To compare the results of all trace length analyses, it is important to verify the differences among the highest values that were obtained from each analysis. For all trace length analyses (measured trace lengths, rectangular sampling windows and circular sampling windows), the values that were obtained for the roof are higher than those for the

east wall. Figure 11 compares the values of  $\mu$  from  $R_c$  and  $CR_{12}$  and  $l_m$  from  $R_m$  (32 m² window of the roof). This figure shows a considerable difference in the mean trace length values from each analysis, where the rectangular sampling windows have higher values for both  $F_1$  and  $F_2$ .

**Frequency, spacing and trace density**

The frequency of discontinuities can be defined as the number of discontinuities per unit volume (3D analysis), the number of discontinuities per unit area (2D analysis) or the number of discontinuities per unit length (1D analysis). Although the first definition is the most representative for a rock mass, it is not possible to perform 3D sampling in geological surveys.

In most practical cases, the discontinuities of a given set are sampled by counting the number of traces that intercept the scanlines (Priest 1993). In this case, the analysis is one dimensional, which gives the linear frequency ( $\lambda$ ) of a discontinuity set, and the inverse of  $\lambda$  is the discontinuity set spacing ( $S$ ). If the scanlines are not oriented perpendicular to the traces in the rock face, the frequency (or spacing) must be corrected by the following expression (Priest 1993):

$$\lambda_\theta = \lambda \cos \theta \tag{9}$$

where  $\lambda_\theta$  is the observed scanline and  $\theta$  is the angle between the scanline and the perpendicular direction of the traces.

Figure 12a shows the position of the scanlines that were used to sample the frequency and spacing for  $F_1$  and  $F_2$  in

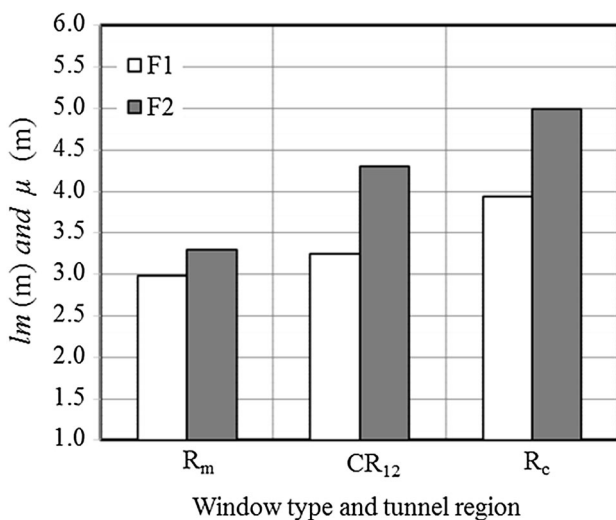


**Fig. 11** Comparison of the highest values obtained from measured and estimated trace lengths (for circular and rectangular sampling windows)

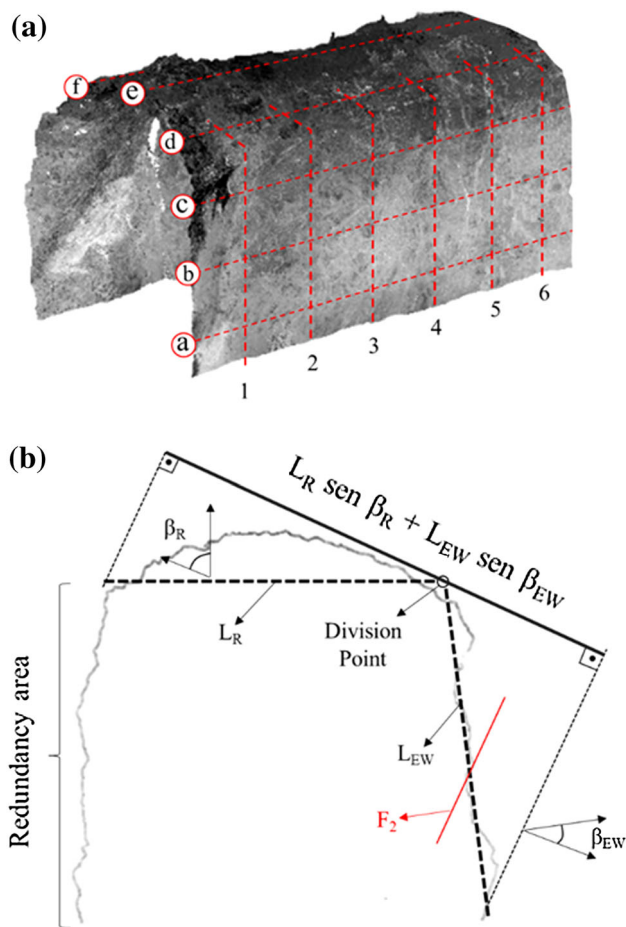


**Fig. 12** a Distribution of the scanlines for  $F_1$  and  $F_2$  on the tunnel, b frequency correction for  $F_2$  from two scanlines ( $L_R$  and  $L_{EW}$ ) with different orientations

the point cloud. In each case, the scanlines must be positioned by considering the best sample direction (the highest number of trace intercepts). Two aspects must be analyzed before obtaining the scanline samples: the variation in the angle ( $\beta$ ) between the rock face (for each approximated planar surface of Fig. 8) and the discontinuity normal vectors (i.e., the orientation bias) and the variation in the rake of traces in each approximated planar surface (which results in one angle  $\theta$  for each surface for each discontinuity set).

Because  $F_1$  is almost perpendicular to the tunnel axis, the orientation of the scanlines is parallel to the axis (see Fig. 12a). In turn, for  $F_2$ , the best sample direction is limited to the tunnel diameter. To better use the available tunnel space, intercept counting is performed using two scanlines, one for the east wall (with length  $L_{EW}$ ) and another for the roof (with length  $L_R$ ), as shown in Fig. 12b. Thus, the true frequency of  $F_2$  is estimated from each pair of scanlines as follows:

$$\lambda = \frac{N_{EW} + N_R}{L_{EW} \sin \beta_{EW} \cos \theta_{EW} + L_R \sin \beta_R \cos \theta_R} \tag{10}$$

where  $N_{EW}$  and  $N_R$  are the numbers of discontinuities that are intercepted in scanlines  $L_{EW}$  and  $L_R$ , respectively;  $\beta_{EW}$  and  $\beta_R$  are the acute angles between the discontinuity set normal and the rock face normal for the east wall and the roof (both approximated for planar surfaces), respectively; and  $\theta_{EW}$  and  $\theta_R$  are the angles described in Eq. 9 when considering the rake variation in each planar surface. To avoid data redundancy in  $F_2$ , only one of the two walls is sampled with scanlines (Fig. 12b). For  $F_1$  fractures, the frequency is also corrected from the angles  $\beta$  and  $\theta$ ; however, because the scanlines are not split in this case, Eq. 10 is reduced to

$$\lambda = \frac{N}{L \sin \beta \cos \theta} \tag{11}$$

where  $N$  is the total number of intercepted discontinuities and  $L$  is the total length of the scanline. Tables 3 and 4 show the results of the frequency and spacing estimation for  $F_1$  (scanlines from a to f in Fig. 12a) and  $F_2$  (scanlines from 1 to 6 in Fig. 12a), respectively.

In the 2D analysis, discontinuity traces are sampled in the rock face areas. The fracture trace density is defined as the mean number of trace centers per unit area (Mauldon 1998). Although it appears simple, it is not possible to identify the trace centers when one or both ends of the traces are censored. In an attempt to overcome this problem, Kulatilake and Wu (1984b) developed a method to estimate the trace density in rectangular sampling areas based on the probability of midpoints (of dissecting and transecting traces) being found within the window. However, this method demands outcrops (sampling areas) where traces that end outside the sampling window can be observed, as in a recent application by Wu et al. (2011). Thus, in small-diameter tunnels (as in this case), this method may not be applicable if it is not possible to observe the entire length of transecting or dissecting traces (mainly for  $F_1$  traces in the present work) in an area with an identical orientation as the sampling window. Mauldon (1998) and Mauldon et al. (2001) developed an end-point estimator of trace density ( $\rho$ ) with the following expression:

$$\rho = \frac{1}{2A} (N - N_T + N_C) = \frac{m}{2A} \tag{12}$$

where  $A$  is the area of the sampling window. The main advantages of this estimator are its independence of both trace length and trace orientation distributions when applied to rectangular or circular sampling windows and its simplicity. However, as observed by Wu et al. (2011), the development of Eq. 12 does not include a contribution

**Table 3** Frequency calculation for  $F_1$

Scanline	$N$	$L$ (m)	$\sin \beta$	$\cos \theta$	$\lambda$ (1/m)	$\bar{\lambda}$ (1/m)	$S$ (m)	$\bar{S}$ (m)
EW								
a	10	8	0.99	0.87	1.44	1.49	0.69	0.67
b	10				1.44		0.69	
c	11				1.59		0.63	
R								
d	19	8	0.98	0.99	2.44	2.10	0.41	0.48
e	17				2.19		0.46	
f	13				1.67		0.60	

**Table 4** Frequency calculation for  $F_2$

Scanline	$N_{EW}$	$N_R$	$L_{EW} = L_R$ (m)	$\sin \beta_{EW}$	$\sin \beta_R$	$\cos \theta_{EW}$	$\cos \theta_R$	$\lambda$ (1/m)	$S$ (m)
1	4	11	4	0.56	0.91	0.96	0.98	2.63	0.38
2	9	9						3.15	0.32
3	8	10						3.15	0.32
4	7	11						3.15	0.32
5	8	11						3.33	0.30
6	7	11						3.15	0.32
$\bar{\lambda}$ (1/m) and $\bar{S}$ (m)								3.09	0.32

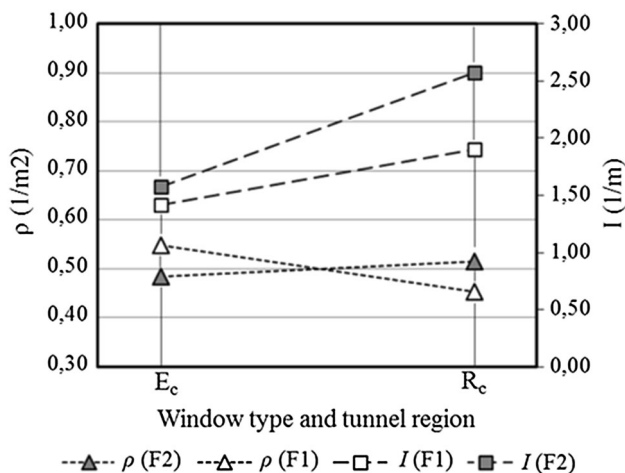


**Fig. 13** Variation in density and intensity of  $F_1$  and  $F_2$  in rectangular sampling windows

from the transecting traces (see Mauldon 1998; Mauldon et al. 2001), which may result in underestimates of the trace density.

Figure 13 shows the estimated densities for the rectangular windows (only  $E_c$  and  $R_c$ ) that were computed using Eq. 12 for  $F_1$  and  $F_2$ . Figure 13 also shows the intensity ( $I$ ) values (calculated as the product  $\rho \times \mu$ ) for the identical windows. The density of  $F_1$  calculated in  $R_c$  can be verified as being lower than the one in  $E_c$  because the transecting traces increase in the roof region (see Fig. 7b). However, the intensity values are always higher in  $R_c$ .

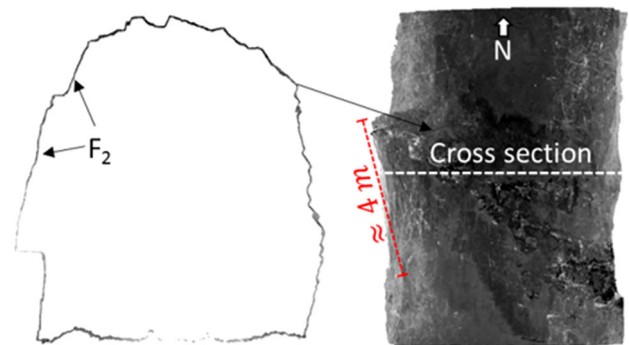


**Fig. 14** Block failure in the west wall

### Discussion and application

The trace map in Fig. 7b shows a discrepancy amongst the west wall, east wall and roof. This result was expected for  $F_2$  fractures because of the orientation bias (Fig. 4), mainly in the highest parts of the west wall, where the rock face dip decreases, becoming almost parallel to  $F_2$ . However,  $F_1$  is absent from the middle to the south portion of the west wall because of a significant block failure (Fig. 14) that generated a flat surface along two  $F_2$  planes. Discontinuity sampling in such sections is impaired, and it thus may be better to avoid these sections when performing frequency and trace length sampling. The differences between mean trace lengths that were observed in sampling windows from the roof and east wall can indicate that fractures may be longer in one direction compared to the other. However, in



the authors opinion, this correlation cannot be immediately claimed if this difference can also (and perhaps even more likely) occur because of the differences in stability of the roof and walls, considering that most unstable regions may result in more continuous exposures of the traces. Therefore, in this case, the discontinuity parameters that were obtained from the roof can be considered to be the most representative. There are several situations wherein the parameters may be different, for example, in horizontal layered sedimentary rocks, where a single flat banding plane may define the tunnel roof; in this case, the walls may be a better choice for the discontinuity analysis. However, it is always possible to verify the best sampling region in the tunnel using 3DTLS images.

The method proposed by Wu et al. (2011) using the estimated parameters  $A$  and  $B$  allows one to estimate the mean trace length for non-vertical surfaces by considering the rake ( $\varphi$ ) variation. To apply the method proposed by Mauldon (1998) for rectangular windows, the rake variations must be visually inferred to estimate the deterministic values of  $A$  and  $B$ . This procedure may be difficult in real geological mapping when a discontinuity set of sparse orientations results in excessive rake variability (as observed for  $F_1$  in this case). However, circular sampling windows (Mauldon 1998; Zhang and Einstein 1998) simplify the analysis if the trace orientation does not interfere with the estimates of  $\mu$ . Despite their attractive practicality, in tunnels (mainly those with small diameters), the size of these windows is limited, which leads to samples that may not represent the entire area. Furthermore, as suggested by Wu et al. (2011), the formulation of Eq. 6 does not consider the influence of relative frequencies (i.e., the rake variations), which implies that it cannot be used to estimate the mean trace length of an identical set from different rock face orientations. In the presented results (Fig. 9a, b), the circular window does not reveal as large of a difference in  $\mu$  between samples  $CE_{12}$  and  $CR_{12}$  as that observed between  $E_c$  and  $R_c$  for rectangular windows. However, for both  $F_1$  and  $F_2$ , the lengths of the rectangular windows in the perpendicular direction of the traces, i.e.,  $(wB + hA)$  in Eq. 1, are smaller for the roof than for the east wall because of the relative frequencies, and the values of  $\mu$  for the roof were expected to be higher. Note that these differences can be substantially more discrepant in other situations with great differences in trace rakes between the roof and the wall (e.g., fractures with the same dip direction as  $F_1$  but with sub-horizontal dips). Therefore, the method proposed by Kulatilake and Wu (1984a) and Wu et al. (2011) appears to be more suitable for unbiased mean trace length estimates in tunnels, where the rock face assumes different orientations.

Here, it was possible to estimate the unbiased SD  $\sigma \approx 0.5\mu$  from the covariance of the measured trace length ( $COV_m$ ) by applying the methodology proposed by Zhang

and Einstein (2000) but using rectangular sampling windows instead of circular ones. Note that with the unbiased  $\sigma$  and  $\mu$  values,  $f(l)$  (probability distribution function of true, or unbiased, trace lengths) can be completely determined after its distribution form (log-normal, negative exponential, gamma, etc.) is assumed to be identical to  $g(l)$  (probability distribution function of measured, or biased, trace lengths). To determine  $g(l)$ , more trace length data are required, which could be obtained through additional point cloud mapping.

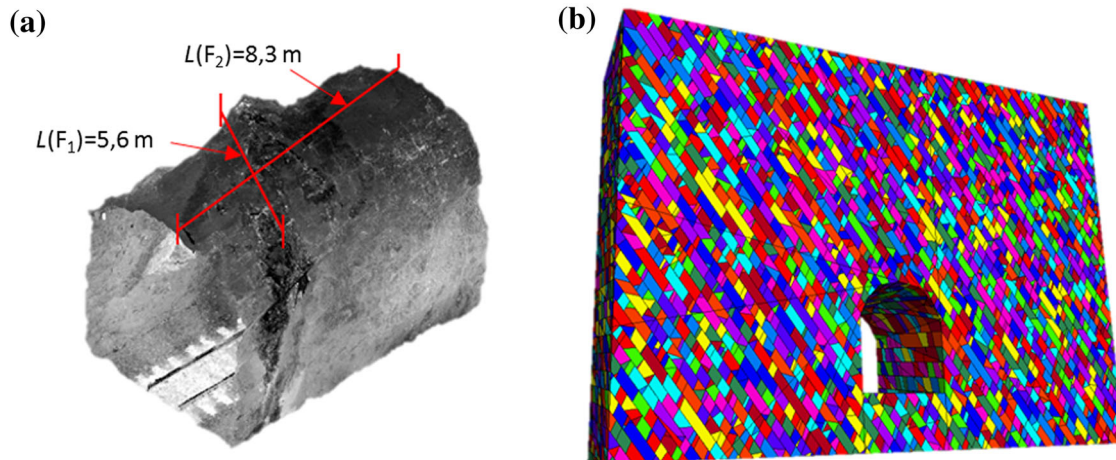
The unbiased areal frequency (density) of traces in the tunnels is a difficult parameter to determine because it is not possible to verify the length of transecting and dissecting traces in an area that is larger than the sampling window. Furthermore, scanline surveys in the point cloud can describe the trace frequency in 1D as long as the respective corrections (from the angles  $\beta$  and  $\theta$ ) are considered. As mentioned above, Eq. 12 (Mauldon 1998) does not consider the contribution of transecting traces in the density estimates. The effect of this simplification can be observed in the  $F_1$  density samples from Fig. 13, where the trace density decreases from  $E_c$  to  $R_c$ , whereas the scanline samples of the roof ( $d$ ,  $e$  and  $f$  in Fig. 12 and Table 3) show frequencies that are clearly higher than the scanlines of the east wall. Limitations of scanlines for frequency sampling may be more critical in cases such as the  $F_2$  set, where the discontinuity and tunnel axis orientations limit the space in which  $F_2$  fractures can appear.

As previously mentioned, foliation ( $S_n$ ) was not analyzed as an impersistent surface because of the genesis characteristics of such geological structures. Certain foliation planes may exhibit a mechanical behavior that is similar to fractures when there is no significant cohesion among the minerals; however, it is difficult to differentiate and delimit such parts of the foliation planes, even in field surveys. Additionally, the assumptions when measuring the mean trace length and frequency via finite trace mapping do not appear reasonable if we consider that the length of the mineral alignment ( $S_n$  planes) can be much longer and much less spaced than observable in the images.

Table 5 summarizes the data that are considered the most representative for this 8-m-long section of the analyzed tunnel with  $\mu$  of  $F_1$  and  $F_2$  obtained from  $R_c$  (Fig. 9a),  $\bar{\lambda}$  of  $F_1$  obtained from scanlines  $d$ ,  $e$  and  $f$  (Table 3), and  $\bar{\lambda}$  of  $F_2$  obtained from scanlines 1–6 (Table 4). The obtained geometrical parameters are useful in many geomechanical applications (geomechanical classifications, numerical modeling, limit equilibrium solutions, etc.), but the mechanical parameters of the joints and intact rock must still be investigated in all applications. An example of an application of all parameters is a block model, which can be generated by 3DEC (Itasca

**Table 5** Representative parameters for the 8-m-long part of the analyzed tunnel

Set	$\bar{\lambda}$ (1/m)	$\bar{S}$ (m)	$\mu$ (m)	$L$ (m)	$P$	Dip (°)	Dip. dir. (°)	1st SD (°)
$F_1$	2.1	0.48	3.93	5.6	0.7	69	166	15.2
$F_2$	3.09	0.32	4.99	8.3	0.6	64	242	5.5
$S_n$	2	0.5	–	–	1	54	80	9.8

**Fig. 15** **a** Estimating the characteristic lengths of the rock mass in the  $F_1$  and  $F_2$  directions, **b** block model generated using 3DEC

Consulting Group 2004). In such models, the orientation and spacing are direct inputs of the program. However, the persistence parameter in the 3DEC code is provided as a percentage of the cutting blocks. As proposed by Kim et al. (2007), this parameter can be estimated as

$$P = \frac{l}{L} \quad (13)$$

where  $l$  is the average joint length, which can be considered here as the estimated mean trace length ( $\mu$ ) for each set, and  $L$  is the characteristic length of the rock mass under consideration for each set, which can be estimated as shown in Fig. 15a. Table 5 also shows the estimated persistence values. For this example, the  $S_n$  planes are 100 % persistent with a spacing of 0.5 m (Table 5). Figure 15b shows the resulting 3DEC model from using the parameters in Table 5.

## Conclusion

Several analyses were performed on a tunnel point cloud that was generated using 3DTLS to determine the important geometrical parameters of discontinuities. The use of point clouds allowed the use of methods for different rock face orientations with identical levels of detail regardless of the position and illumination. However, care must be taken during data acquisition to decrease the number of

occlusions, and during orientation mapping to avoid sampling planes with limited exposures.

The method proposed by Wu et al. (2011) appears to be a good choice for sampling the unbiased mean trace length for different rock face orientations. The difficulty in determining the relative frequencies of traces (imposed by this method) is overcome when 3DTLS is used for discontinuity mapping and when the position of each orientation measurement is known. In general, both the mean trace length and the frequency in the roof are higher than in the east wall, which implies that in a conventional survey in a manually reachable area, the parameters can be underestimated. Moreover, the constancy of the covariance of the measured trace lengths in different rectangular sampling areas could be verified, which allowed us to obtain the unbiased SD. These data are important for characterizing probability distribution functions that will be useful in future works with other parameters.

Although only an 8-m-long section of the tunnel was analyzed in the present work, the applicability of different methodologies of discontinuity analysis was verified in the point cloud. Thus, after the jointed regions of the tunnel (similar to the section presented) are identified in an image, the same methods that were used here can be applied to each region.

**Acknowledgments** The authors would like to thank the company VALE SA and the National Council of Technological and Scientific Development (CNPq) for the logistical and financial support.

## References

- Baecher GB (1980) Progressively censored sampling of rock joints traces. *Math Geol* 12(1):33–40. doi:[10.1007/BF01039902](https://doi.org/10.1007/BF01039902)
- Crosta G (1997) Evaluating rock mass geometry from photogrammetric images. *Rock Mech Rock Eng* 30(1):35–38. doi:[10.1007/BF01020112](https://doi.org/10.1007/BF01020112)
- Cruden DM (1977) Describing the size of discontinuities. *Int J Rock Mech Min Sci Geomech Abstr* 14:133–137. doi:[10.1016/0148-9062\(77\)90004-3](https://doi.org/10.1016/0148-9062(77)90004-3)
- Faro Inc. (2013) SCENE V 5.0, Lake Mary, FL
- Fekete S, Diederichs M, Lato M (2010) Geotechnical and operational applications for 3-dimensional laser scanning in drill and blast tunnels. *J Tunn Undergr Space Technol* 25:614–628. doi:[10.1016/j.tust.2010.04.008](https://doi.org/10.1016/j.tust.2010.04.008)
- Ferrero AM, Forlani G, Roncella R, Voyat HI (2009) Advanced geostuctural survey methods applied to rock mass characterization. *Rock Mech Rock Eng* 42:631–665. doi:[10.1007/s00603-008-0010-4](https://doi.org/10.1007/s00603-008-0010-4)
- Gigli G, Casagli N (2011) Semi-automatic extraction of rock mass structural data from high resolution LIDAR point clouds. *Int J Rock Mech Min Sci* 48:187–198. doi:[10.1016/j.ijrmms.2010.11.009](https://doi.org/10.1016/j.ijrmms.2010.11.009)
- Haneberg WC (2008) Using close range terrestrial digital photogrammetry for 3-D rock slope modeling and discontinuity mapping in the United States. *Bull Eng Geol Environ* 67:457–469. doi:[10.1007/s10064-008-0157-y](https://doi.org/10.1007/s10064-008-0157-y)
- International Society for Rock Mechanics (1978) Suggested methods for the quantitative description of discontinuities in rock masses. *Int J Rock Mech Min Sci Geomech Abstr* 15:319–368. doi:[10.1016/0148-9062\(78\)91472-9](https://doi.org/10.1016/0148-9062(78)91472-9)
- Itasca Consulting Group (2004) 3DEC V 4.1, Minneapolis, MN
- Kemeny J, Turner K, Norton B (2006) LIDAR for rock mass characterization: hardware, software, accuracy and best-practices. In: Proceedings of the workshop on laser and photogrammetric methods for rock face characterization, Golden, CO, pp 49–61
- Kim BH, Cai M, Kaiser PK, Yang HS (2007) Estimation of block size for rock masses with non-persistent joints. *Rock Mech Rock Eng* 40(2):169–192. doi:[10.1007/s00603-006-0093-8](https://doi.org/10.1007/s00603-006-0093-8)
- Kulatilake PHSW, Wu TH (1984a) Estimation of mean trace length of discontinuities. *Rock Mech Rock Eng* 17:215–232. doi:[10.1007/BF01032335](https://doi.org/10.1007/BF01032335)
- Kulatilake PHSW, Wu TH (1984b) The density of discontinuity traces in sampling windows. *Int J Rock Mech Min Sci Geomech Abstr* 21(6):345–347. doi:[10.1016/0148-9062\(84\)90367-X](https://doi.org/10.1016/0148-9062(84)90367-X)
- Lato MJ, Vöge M (2012) Automated mapping of rock discontinuities in 3D lidar and photogrammetry models. *Int J Rock Mech Min Sci* 54:150–158. doi:[10.1016/j.ijrmms.2012.06.003](https://doi.org/10.1016/j.ijrmms.2012.06.003)
- Lato MJ, Diederichs MS, Hutchinson DJ, Harrap R (2009) Optimization of LiDAR scanning and processing for automated structural evaluation of discontinuities in rock masses. *Int J Rock Mech Min Sci* 46:194–199. doi:[10.1016/j.ijrmms.2008.04.007](https://doi.org/10.1016/j.ijrmms.2008.04.007)
- Lato MJ, Diederichs MS, Hutchinson DJ (2010) Bias correction for view-limited lidar scanning of rock outcrops structural characterization. *Rock Mech Rock Eng* 43:615–628. doi:[10.1007/s00603-010-0086-5](https://doi.org/10.1007/s00603-010-0086-5)
- Mah J, Samson C, Mckinnon SD (2011) 3D laser imaging for joint orientation analysis. *Int J Rock Mech Min Sci* 48:932–941. doi:[10.1016/j.ijrmms.2011.04.010](https://doi.org/10.1016/j.ijrmms.2011.04.010)
- Mauldon M (1998) Estimating mean fracture trace length and density from observation in convex windows. *Rock Mech Rock Eng* 31(4):201–216. doi:[10.1007/s006030050021](https://doi.org/10.1007/s006030050021)
- Mauldon M, Dunne WM, Rohrbaugh MB Jr (2001) Circular scanlines and circular windows: new tools for characterizing the geometry of fracture traces. *J Struct Geol* 23:247–258. doi:[10.1016/S0191-8141\(00\)00094-8](https://doi.org/10.1016/S0191-8141(00)00094-8)
- Pahl PJ (1981) Estimating the mean length of discontinuity traces. *Int J Rock Mech Min Sci Geomech Abstr* 18:221–228. doi:[10.1016/0148-9062\(81\)90976-1](https://doi.org/10.1016/0148-9062(81)90976-1)
- Priest SD (1993) Discontinuity analysis for rock engineering. Chapman & Hall, London
- Rocscience Inc. (2006) DIPS V 5.1, Toronto, Ontario
- Slob S, Hack HRGK, Feng Q, Röshoff K, Tunner AK (2007) Fracture mapping using 3D laser scanning techniques. In: 11th congress of the international society for rock mechanics, Lisbon, pp 299–302
- Split Engineering, LCC. (2007) Split-FX V 2.1, Tucson, AZ
- Strouth A, Eberhardt E, Hungr O (2006) The use of lidar to overcome rock slope hazard data collection challenges at Afternoon Creek, Washington. In: 41st U.S. symposium on rock mechanics (USRMS), CO, pp 17–21
- Sturzenegger M, Stead D (2009) Close-range terrestrial digital photogrammetry and terrestrial laser scanning for discontinuity characterization on rock cuts. *Eng Geol* 106:163–182. doi:[10.1016/j.enggeo.2009.03.004](https://doi.org/10.1016/j.enggeo.2009.03.004)
- Sturzenegger M, Stead D, Elmo D (2011) Terrestrial remote sensing-based estimation of mean trace length, trace intensity and block size/shape. *Eng Geol* 119:96–111. doi:[10.1016/j.enggeo.2011.02.005](https://doi.org/10.1016/j.enggeo.2011.02.005)
- Terzaghi RD (1965) Sources of error in joint surveys. *Geotechnique* 15:287–304. doi:[10.1680/geot.1965.15.3.287](https://doi.org/10.1680/geot.1965.15.3.287)
- Umili G, Ferrero A, Einstein HH (2013) A new method for automatic discontinuity traces sampling on rock mass 3D model. *Comput Geosci* 51:182–192. doi:[10.1016/j.cageo.2012.07.026](https://doi.org/10.1016/j.cageo.2012.07.026)
- Wathugala DN, Kulatilake PHSW (1990) A general procedure to correct sampling bias on joint orientation using a vector approach. *Comput Geotech* 10:1–31. doi:[10.1016/0266-352X\(90\)90006-H](https://doi.org/10.1016/0266-352X(90)90006-H)
- Wu Q, Kulatilake PHSW, Tang H (2011) Comparison of rock discontinuity mean trace length and density estimation methods using discontinuity data from an outcrop in Wenchuan area, China. *Comput Geotech* 38:258–268. doi:[10.1016/j.compgeo.2010.12.003](https://doi.org/10.1016/j.compgeo.2010.12.003)
- Zhang L, Einstein HH (1998) Estimating the mean trace length of rock discontinuities. *Rock Mech Rock Eng* 31(4):217–235. doi:[10.1007/s006030050022](https://doi.org/10.1007/s006030050022)
- Zhang L, Einstein HH (2000) Estimating the intensity of rock discontinuities. *Int J Rock Mech Min Sci* 37:819–837. doi:[10.1016/S1365-1609\(00\)00022-8](https://doi.org/10.1016/S1365-1609(00)00022-8)